CrystEngComm

PAPER

View Article Online
View Journal | View Issue

Cite this: *CrystEngComm*, 2015, **17**, 9459

Site selective Cu deposition on Au microcrystallites: corners, edges *versus* planar surfaces†

Gangaiah Mettela[a] and Giridhar U. Kulkarni‡*[b]

Received 6th August 2015,
Accepted 9th November 2015

DOI: 10.1039/c5ce01574j

www.rsc.org/crystengcomm

Among epitaxially grown metal over metal systems, Cu on a Au surface forms a notable exception given the large lattice mismatch (~11.2%). Although widely observed, Cu growth on Au is less understood at both nano and bulk length scales. In this work, we have relied on Au microcrystallites which provide adequate platform to access both the length scales and thus have examined Cu electroless deposition using electron microscopy techniques, on planar as well as corner and edge regions distinctly. Amazingly, the growth at different regions was found to be highly varied; the corners were found to be most active, followed by edges and planar regions. Interestingly, the sharper the corner, the higher the Cu deposition is. Importantly, both Au{111} and Au{100} facets could be explored simultaneously, using a routine electron microscope.

1. Introduction

Heterometallic systems are interesting due to their enhanced chemical stability and catalytic activity.[1] In recent years, these interfaces are being revisited equipped with new synthetic procedures and advanced microscopy tools.[2–6] Various physical and chemical methods have been employed for conformal growth of one metal over another, where the growth can be epitaxial or non-epitaxial. Usually, epitaxial growth takes place when the lattice mismatch between the participating metals is below 5%, Au/Ag,[6] Au/Pd[7] and Pd/Pt[4] being well known examples. Metals with higher lattice mismatch (such as Pd/Ag) do not tend to exhibit epitaxial growth; however, Cu epitaxial growth on various noble and semi-noble metal surfaces is a clear exception. For instance, despite higher lattice mismatch, Cu can epitaxially grow on Pd (7.1%)[2] and Au (11.2%) due to favorable underpotential deposition (UPD)[5,8–10] and higher Cu–M bond strength (M = Pd and Au, *etc.*).[11] Sieradzki *et al.* have reported that the strain generated due to the lattice mismatch gets relaxed through the generation of misfit dislocation.[12] Using scanning tunneling microscopy (STM), Magnussen *et al.*[13] studied the Cu growth on a bulk Au{111} surface by electrochemical deposition and ascribed the growth mode to be Stranski–Krastanov (SK), *i.e.* wetting layer and island formation take place simultaneously. On the contrary, Grillo *et al.*[14] in their STM study have reported Frank–van der Merwe (FvdM) type growth for vacuum deposited Cu (layered by layer type growth). In the abovementioned studies, Cu deposition was monitored only on planar surfaces, while the nature of growth at corners and edges was not examined. Bulk single crystals used in such studies offer extended surfaces but make edges and corners practically inaccessible. As regards nanoparticles, Au nanocrystallites of different shapes have been tried out in solution-based epitaxial Cu deposition. Due to the finite size of nanoparticles, contributions from corners and edges become very significant.[15] The relevant growth modes (FvdM[16] and Tsuji–Ikedo type growth[17]) have been identified using high resolution transmission electron microscopy (TEM). In spite of high resolution imaging, finer details relating to shape and crystallographic orientation of the deposited Cu islands could not been discerned.[16,17] In other words, the nature of growth on the planar nanoparticle surface as against those on corners and edges is usually not easily distinguishable, although the nanoparticle as a whole is accessible in microscopy. The issue therefore appears to be around the length scale associated with the bimetal system, single crystals and nanocrystallites being at extreme ends of the scale. An intermediate length scale pertaining to microcrystals should provide the right platform to access all three simultaneously, planar surfaces, corners and edges, while being able to distinguish and study the nature of growth at each region. Well faceted Au microcrystals grown using a procedure developed in the laboratory indeed prompted this study.[18–20] To grow Cu epitaxially, an electroless deposition method was adopted,[21] so that external influences are avoided. The extent of Cu deposition on different

[a] *Thematic Unit of Excellence on Nanochemistry and Chemistry and Physics of Materials Unit, Jawaharlal Nehru Centre for Advanced Scientific Research (JNCASR), Jakkur P.O., Bangalore 560 064, India*
[b] *Centre for Nano and Soft Matter Sciences, Jalahalli, Bangalore 560013, India. E-mail: guk@cens.res.in*

† Electronic supplementary information (ESI) available: Synthetic conditions, XRD, EDS and TEM analysis. See DOI: 10.1039/c5ce01574j

‡ On lien from JNCASR, Bangalore.

regions of the microcrystallite was monitored using electron microscopy (SEM) and the elemental identity by energy dispersive X-ray analysis (EDS). Where relevant, TEM and X-ray diffraction (XRD) techniques have also been employed. The effect of the microcrystal size on Cu deposition has also been investigated. The present study thus not only provides a satisfactory explanation for Cu growth on Au but also puts all ambiguities to rest, related to lattice mismatch and epitaxy.

2. Experimental section

Materials

Gold chloride ($HAuCl_4$), tetraoctylammonium bromide (ToABr), copper sulphate ($CuSO_4$), sodium potassium tartrate ($KNaC_4H_4O_6{\cdot}4H_2O$), sodium hydroxide (NaOH) and toluene were used. All reagents were purchased from Spectrochem, India. Water used in this study was double distilled and deionized. Si substrates were cleaned with water, IPA, and toluene and dried under N_2 gas.

Synthesis of Au microcrystallites

Au microcrystallites were prepared by using one of our recent reports. Briefly, to a 100 μL of $HAuCl_4$ (25 mM), 300 μL of ToABr in toluene (50 mM) was added and stirred for 5 min. 100 μL of organic layer was coated on a Si substrate and heated at 135 °C on a hot plate in air. After growing Au microcrystals, they were washed with toluene to remove any residual precursor and dried with flowing nitrogen.

Cu electroless deposition

Copper plating solution contains solutions A and B. Solution A was prepared by dissolving $CuSO_4$ (3 g), sodium potassium tartrate (14 g) and NaOH (4 g) in 100 ml of distilled water. Solution B was an aqueous solution of formaldehyde (37.2 wt%). Solutions A and B were mixed in the volume ratio of 5 : 1. For Cu electroless deposition, Au microcrystallites were dipped in plating solution. The process was halted at different times by taking out the sample from the solution. The obtained Au/Cu crystallites were characterized using SEM, EDS, TEM and XRD techniques.

Characterization

Scanning electron microscopy (SEM) was performed using a Nova NanoSEM 600 equipment (FEI Co., The Netherlands). Energy dispersive spectroscopy (EDS) mapping was performed using an EDAX Genesis V4.52 (USA) attached to an SEM column. Atomic force microscopy (AFM) experiments were carried out using a Bruker diInnova Scanning Probe Microscope with a Nanodrive controller. Imaging has been done in tapping mode. TEM measurements were carried out using a JEOL-3010 instrument operating at 300 kV. XRD measurements were performed using a PANalytical instrument (Cu Kα, 1.5406 Å; scan rate, 1°/3 min).

3. Results and discussion

Au microcrystals were prepared using a method reported recently.[18,19] Briefly, a AuToABr complex is prepared by the stabilization of $(AuCl_4)^-$ with tetraoctylammonium bromide (ToABr) in toluene (~50 mM). A few drops (~30 μL) of AuToABr solution was drop-coated on a Si substrate and thermalized on a hot plate at 135 °C in air for 1 h. The samples were washed with toluene to dissolve the unreacted precursor. Among the obtained Au microcrystals, hexagons and triangles occurred more frequently, while cuboctahedra, pentatwinned nanorods and decahedra form the minor products.[20] The width of these crystals ranges from ~0.7 to 80 μm. The crystallites exhibit well defined smooth facets, assignable to {111} and {100}.[20] One such Au microcrystal is shown in Fig. 1a. In hexagons, triangles and cuboctahedra, top and bottom facets are made of {111} facets, whereas the {100} and {111} construct the side facets (Fig. 1b and S1†).[20] These crystallites exhibit sharp corners with interior angles of 120° (hexagon) and 60° (triangle) (see Fig. S2†). To grow Cu epitaxially on Au microcrystals, the electroless deposition method is preferable as the process will be guided by the nature of the host surface rather than an external electric field.[13] For the same reason, the crystallites were used without any surface modification. The deposition involved the reduction of Cu(II)–tartrate in alkaline medium with formaldehyde onto the Au microcrystals.[22] Here, Au being an active catalyst for oxidation of formaldehyde in basic medium is clearly an advantage.[23] Hence, Cu deposition takes place rapidly on the Au crystallites. The reduction of Cu(II) can be described by the following equations:[22]

$$HCHO + OH^- \rightarrow HCOO^- + 1/2\ H_2 + 2e^- \quad (1)$$

$$Cu(II) + 2e^- \rightarrow Cu(0) \quad (2)$$

For electroless deposition of Cu, as-prepared Au microcrystals were immersed in the copper plating solution. A series of intermediate products were captured by halting the Cu deposition at different times. After plating, the samples were washed with water and ethanol and dried under N_2 gas. Cu growth on Au surfaces has revealed several interesting aspects as discussed below. In the very initial stages, Au surfaces become somewhat rough before distinct deposition can be observed, which may be attributed to the Cu wetting layer (see EDS in Fig. S3†). After 4 min exposure to the plating solution, the Au{111} facets get covered with triangle and hexagonal shaped islands (Fig. 1c and d), while on Au{100} facets square shaped islands are seen (Fig. 1f and g), and all the islands are composed of Cu as evident from EDS analysis (see the spectrum in Fig. 1f). Interestingly, the interior angles of Cu triangles and hexagons are ~60° and ~120°, respectively, which essentially reflect the symmetry of the Au{111} facet itself. Further, the angles between two adjacent Cu islands are ~60° and 120°, indicating that the space between Cu islands can be filled by either a triangle (for 60° gap) or a

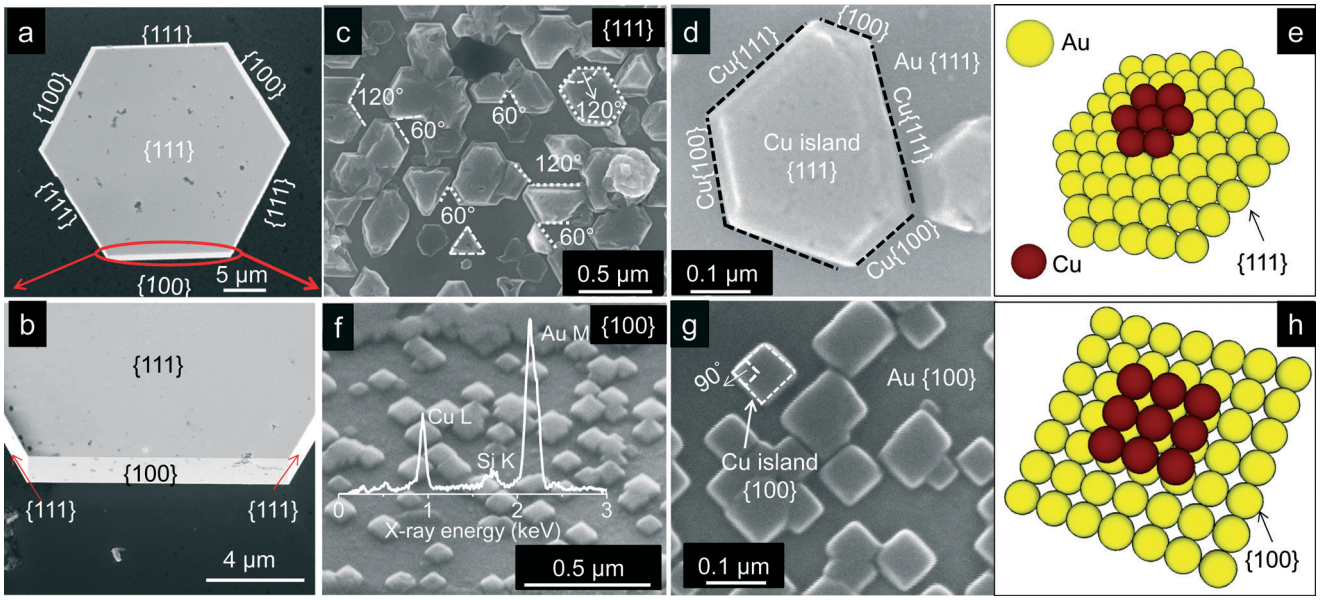

Fig. 1 (a, b) SEM images of a Au microcrystal at different magnifications before Cu deposition. SEM images depicting the shape of Cu islands formed on Au{111} (c and d) and Au{100} (f and g) facets. Pictorial representation of Cu islands on Au{111} and {100} facets are shown in (e) and (h), respectively. The corresponding EDS spectrum collected from Cu islands is shown on the top of image f.

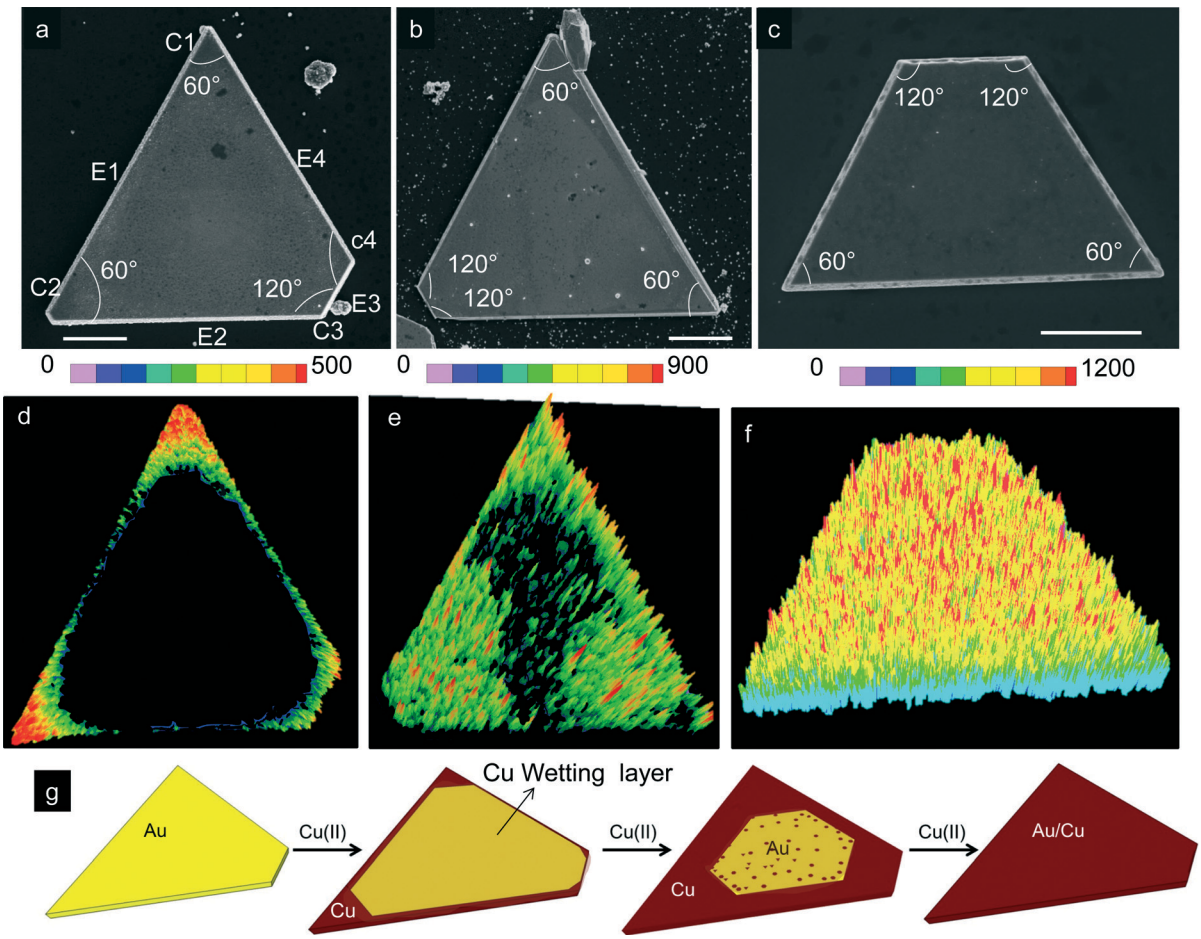

Fig. 2 (a–c) SEM images of trapezoid Au crystals after Cu deposition for (a) 4, (b) 8 and (c) 12 min. (d–f) Contour plots illustrate the distribution of the Cu L signal across the Au crystallites shown in a, b and c, respectively. (g) Schematic illustration of site selective Cu deposition on Au microcrystals. Scale bar, 10 μm.

hexagon (120°) (Fig. 1c), clearly indicating epitaxial relation in the growth. This observation is similar to that made by Magnussen *et al.* based on *in situ* STM studies of the surface.[13] After prolonged deposition, the size of the Cu islands increased up to ~500 nm (Fig. S6†), and the average height increased up to ~140 nm (Fig. S5†) to eventually form a continuous film (Fig. S6†). Similarly on the {100} facets, square shaped Cu islands with an interior angle of 90° closely pack themselves (Fig. 1f and g). Like the parent Au crystallites, the Cu crystallites (islands) are seen enclosed with well-defined facets; those formed on Au{111} are enclosed with {111} and {100} facets (Fig. 1d), while those on {100} follow the substrate morphology itself (Fig. 1g).[5] The above observations are schematically illustrated in Fig. 1e and h.

It appears that Cu initially forms a wetting layer as shown by EDS and increases in surface roughness (see Fig. S3 and S4†) before well-defined islands could grow with specific relation to the geometry of the underlying Au facet. This growth therefore closely resembles the SK (Stranski–Krastanow) mode,[5] which is also understandable following the three rules introduced by Fan *et al.* for bimetal interfaces.[3] Because of lower atomic radius and electronegativity values of Cu (0.138 nm, 1.9 eV) compared to those of Au (0.144 nm, 2.54 eV) and higher Au–Cu bond strength, Cu can easily wet the Au surface forming few layers.[16] As the deposition advances, island-like Cu crystallites are formed as shown in Fig. 1. Our observations on Au microcrystals differ from those made by Tsuji *et al.* and Yoshida *et al.* on Au nanocrystals who reported layer type growth mode.[16,17] The nanocrystal surface being relatively more active, only layer type deposition may be favored. Examples of SEM and EDS mapping of Au trapezoid microcrystals with top {111} facet hosting 60° and 120° corners are shown in Fig. 2a–f. After 4 minutes of electroless reaction (Fig. 2a), the extent of Cu deposition is found to be relatively high at the 60° corners compared to that at the 120° corners, and interestingly, no deposition is seen in the center (see Cu L contour image in Fig. 2d). From the 60° corner (C1) seen at the top of the image, the deposition extends up to ~7.5 μm inwardly on the {111} facet, which is slightly less (5.3 μm) for the left 60° corner (C2) presumably due to its lesser sharpness. Importantly for the 120° corners (C3 and C4), these values are much lower (1.5–1.7 μm). The above observations clearly indicate that the propensity of Cu deposition is varied around the given Au{111} facet implying a lower Au–Cu lattice on the angle enclosed at the corner. The {111} facet exhibits corners with angles of 120° and 60°, and the corresponding CN values are 6 and 5.

The Au–Au bond length is mismatch at corners and edges, else the observed deposition would have been uniform all over the surface. It may be noted that these observations are quite different from what is reported in the literature. In earlier studies on large Au single crystal surfaces (typically few mm to cm), the corners and edges have not been examined.[5] In the case of nanocrystallites, Tsuji *et al.* have reported non-uniform deposition of Cu and Ni on Au nanocrystallites,[16,24] which was attributed to higher lattice mismatch. However, there has been no detailed study that deals with the participation of corners and interior angles of facets of nano/microcrystallites in obtaining hetero-metallic systems. In our study, this aspect has come out quite clearly. The above observations may be explained based on local reactivity as well as lattice mismatch between the Au surface and the incoming Cu. In general, surface atoms have lower coordination number than the bulk atoms (CN, 12).[25,26] The CN value for surface Au atoms on the {111} and {100} facets is 9 and 8, respectively. At edges, it is 7, and at the corners, it can be even lower, depending on the angle extended by the corner (Fig. 3b). Accordingly, the order of Au–Au bond length is as follows: bulk (2.88 Å) > surface Au{111} (2.84 Å) > surface Au{100} (2.82 Å) > edge (2.80 Å) > corner with 120° (2.78 Å) and corner with 60° (2.77 Å).[25–28] It is evident that the mismatch with respect to the Cu–Cu bond length (2.56 Å)[29] should follow the same order: 11.2% (bulk), 9.85% (surface {111}), 9.21% (surface {100}), 8.57% (edge), 7.91% (120° corner) and 7.58% (60° corner) (Fig. 3a).[25] A similar trend has been obtained in the DFT study.[27] From these considerations, one may expect that the propensity of Cu deposition should increase in the same order. It appears that as more and more Cu is deposited at the corners and edges, the growth towards the central region is essentially independent of the underlying substrate, which depends rather on interfacial strain.[30] During the epitaxial growth, the adatoms may undergo surface diffusion on the Au surface. The newly reduced Cu atom at the corners is likely to diffuse to the edge and planar surfaces,[31,32] instead of getting added to the existing Cu nuclei. However, such diffusion is a slow process as the Cu deposition takes place at room temperature. This kind of site selective Cu deposition on Au has been observed for the first time, to the best of our knowledge. After 8 minutes, Cu deposition extends gradually to the center of the microcrystal (Fig. 2b and e), to eventually cover the whole facet (Fig. 2c and f). After 12 minutes, Au crystallites of different shapes are fully covered by Cu (Fig. 4). The progress of Cu deposition is illustrated in the schematic in Fig. 2g. We have observed a similar trend in a hexagonal shaped Au microcrystal hosting top {111} facet with 120° corners. Cu deposition started at corners and edges and propagated to the center of the Au hexagon (see Fig. S7†). Therefore, it is understandable that Cu deposition selectively commences from the sharp corners, followed by edges, and progresses towards the center of the microcrystal (Fig. 2 and S7†).

Besides the crystal shape, the size also plays a role in Cu deposition (Fig. 5). For a crystallite size of ~52 μm after 15 min exposure to electroless plating solution, the atomic ratio of Cu to Au as measured by EDS was <0.1, while the value was ~43 for a 0.7 μm crystallite (Fig. 5a–e and S8†). It is evident that the Cu to Au ratio increases as the width of the Au plate decreases. Here, a higher atomic ratio arises due to limited penetration of the e-beam into Au due to the thick Cu overlayer and thus stands for relative Cu thickness. For the size range studied, the thickness of the Au crystallites varies in a narrow size from 200 nm (small Au

a

Coordination Number (CN) [28]	12	9	8	7	6	5
Location	Bulk	(111) surface	(100) Surface	Edge	corner (120 deg)	corner (60 deg)
Au-Au Bond length (Å) [25, 26]	2.88	2.84	2.82	2.80	2.78	2.77
Mismatch (%)	11.11	9.85	9.21	8.57	7.91	7.58

b

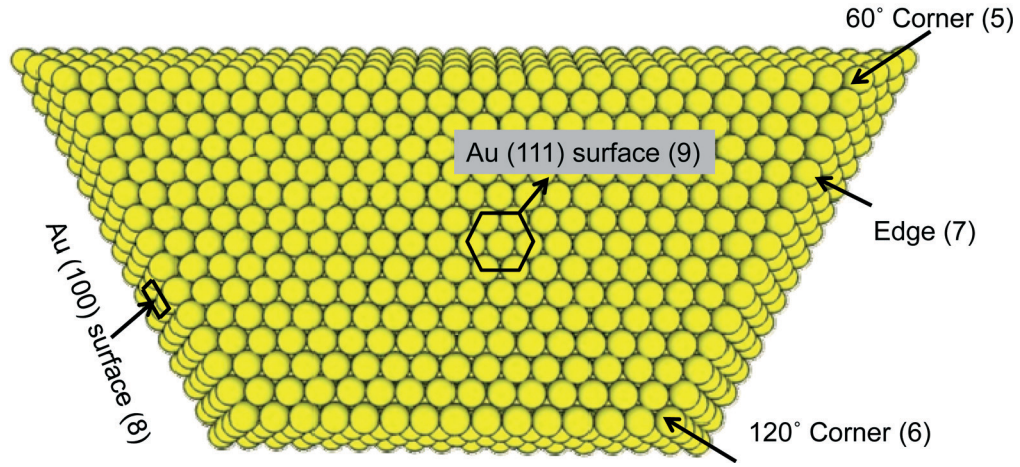

Fig. 3 (a) Calculated lattice mismatch for Cu at various sites of Au microcrystallites by considering the bulk Cu–Cu bond length of 2.56 Å (ref. 29). Au–Au bond lengths are taken from ref. 25 and 26. (b) Schematic illustration of various sites on a trapezoid with the respective coordination number (CN) in brackets.

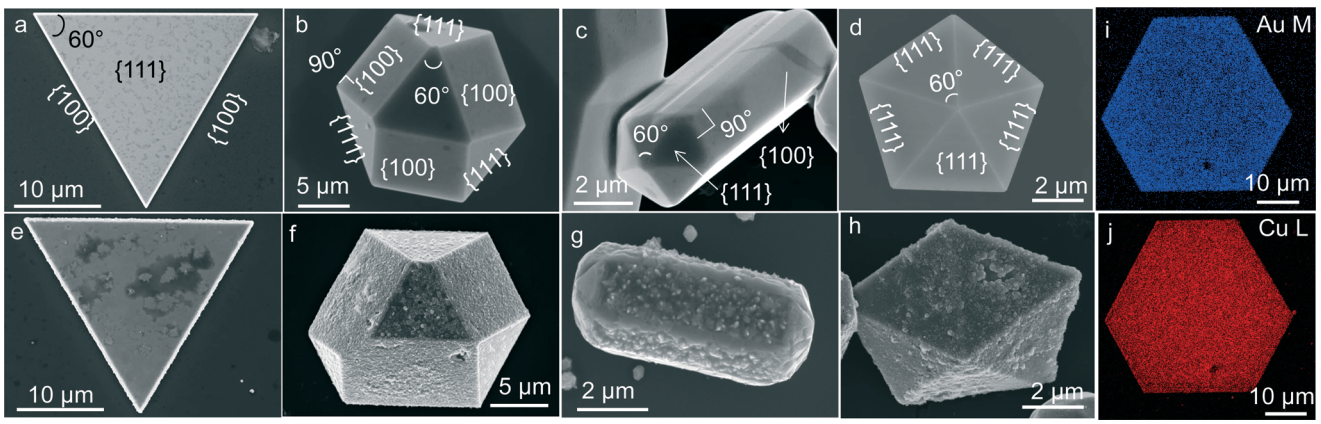

Fig. 4 SEM images of Au microcrystals of different shapes before and after Cu deposition; triangle (a, e), cuboctahedron (b and f), penta-twinned nanorod (c and g) and decahedron (d and h). The interior angles of {111} and {100} facets of various geometries have been assigned. (i, j) Au M and Cu L maps of the hexagon.

crystallites, <1 μm wide) to 800 nm (large Au crystallites, ~50 μm wide) (Fig. S9†). Although nano- and micro-crystallites possess similar internal angles, Cu deposition is relatively higher on nanocrystallites due to their finite size. The separation between edges increases with the size of the crystallites. Hence, in the case of microsize Au crystals, the time needed for the complete deposition is higher than in the case of nanocrystallites. In the given size range, the thickness of the Au crystallite does not seem to influence the overall Cu growth rate. Further, TEM analysis has also confirmed the epitaxial growth of Cu on Au crystallites. The TEM image and ED pattern of Au/Cu core–shell nano-crystallites are shown in Fig. 5f and g. Due to the higher atomic number of Au (Z = 79), the core appears much

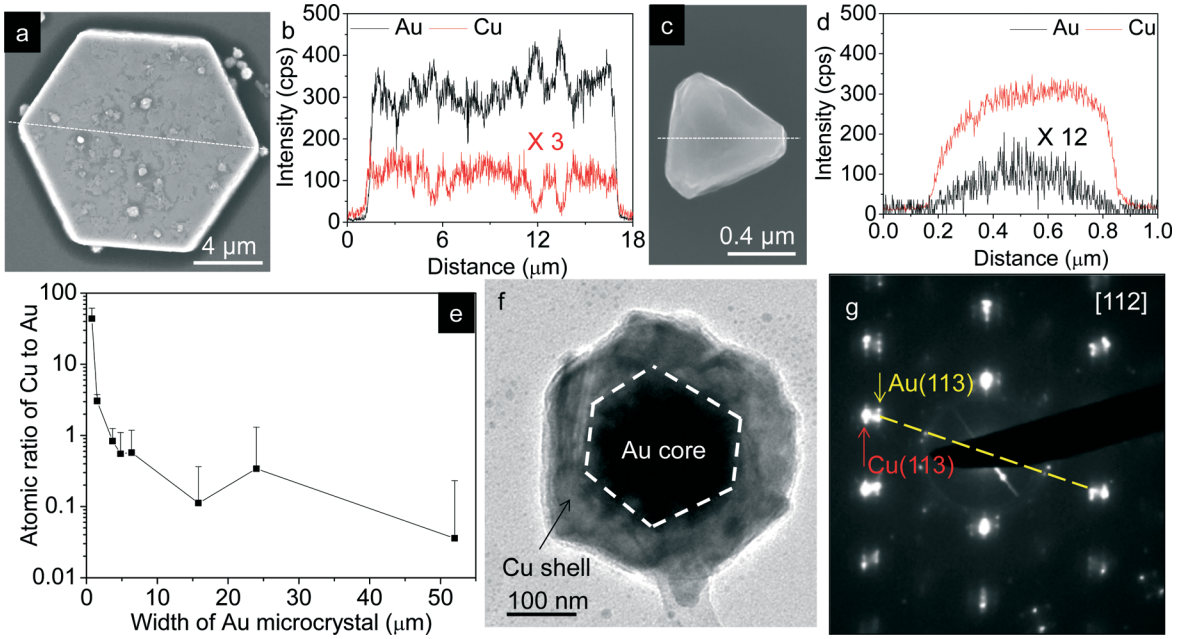

Fig. 5 (a and c) SEM images of Au/Cu core–shell microcrystals and (b and d) line mapping along the lines drawn in a and c. (e) at% ratio of Cu to Au along the width of Au microcrystallites. (f, g) TEM image and ED pattern obtained from the Au/Cu nanocrystallite. In ED, yellow and red arrows represent diffraction spots from Au and Cu lattices, respectively.

brighter than the Cu shell (z = 29).[33,34] As evident from the TEM image (Fig. 5f), Au/Cu core–shell nanocrystallites follow the geometry of the Au crystallite; it also confirms the conformal coverage of Cu on Au nanocrystallites. The ED pattern of the Au/Cu triangle obtained from center regions along the [112] zone axis consists of reflections of Au and Cu (Fig. 5g), while the ED from the edge is assignable to only Cu spots (Fig. S10†). As shown in the ED pattern (Fig. 5g), Au and Cu are similarly oriented irrespective of the shape of the Au core. The allowed reflections of Au and Cu are collinear, indicating that Cu has grown epitaxially on Au despite the larger lattice mismatch (11.2%) between Au and Cu. The Cu islands attached to the Au core are covered with {111} facets (Fig. S10†). Finally, XRD patterns recorded from pristine Au and Au/Cu are dominated with the {111} reflection of Au due to the preferential orientation of the majority of the crystallites (Fig. S1†). Au/Cu core–shell microcrystallites exhibit a weak reflection at ~43.5° assignable to Cu{111}, while other reflections of Cu are not seen in the XRD pattern. Importantly in the XRD pattern, neither new peaks nor deformation in any of the peaks is observed, indicating the absence of Au–Cu alloy formation, and the core/shell formation does not affect the lattice parameters of Au and Cu (see Table S1†).

4. Conclusions

In conclusion, the present study addresses the epitaxial growth of Cu on a Au surface employing Au microcrystallites of different shapes in a simple electroless deposition method. Cu growth involved the formation of a wet layer on Au surfaces followed by islands, which is the classical SK mode. The shape of the Cu islands follows the crystal nature of the underlying surface; hexagonal, triangle and square shaped Cu islands have been observed on Au{111} and Au{100} facets, respectively. For the first time, the role of the surface site, planar, edge or corner, on Cu epitaxial growth is demonstrated here. Cu deposition was found to be dependent on the local reactivity of the sites rather than the shape of the crystallites. It is clearly shown that Cu deposition commenced at sharper corners (60°) followed by broader 120° corners and edges and, finally, at planar sites. We have also studied the size effect on Cu deposition. Cu deposition is relatively slower on larger Au crystallites than on smaller crystallites. The work demonstrated here is, in principle, extendable to other noble metals with high lattice mismatches, for example, Ag/Cu and Au/Ni systems.

Acknowledgements

The authors thank Prof. C. N. R. Rao for his constant encouragement. The generous support from Nanomission DST, India is gratefully acknowledged. We thank Ms. Summayya Kouser and Ms. Nisha Mammen for useful discussion. The authors also thank Dr. Basavaraja, Mrs. Usha and Mr. Anil for AFM, TEM and XRD measurements. G. M. thanks CSIR, India for financial assistance.

References

1 R. Ghosh Chaudhuri and S. Paria, *Chem. Rev.*, 2012, **112**, 2373–2433.

2 M. Jin, H. Zhang, J. Wang, X. Zhong, N. Lu, Z. Li, Z. Xie, M. J. Kim and Y. Xia, *ACS Nano*, 2012, **6**, 2566–2573.
3 F. R. Fan, D. Y. Liu, Y. F. Wu, S. Duan, Z. X. Xie, Z. Y. Jiang and Z. Q. Tian, *J. Am. Chem. Soc.*, 2008, **130**, 6949–6951.
4 K. Cao, Q. Zhu, B. Shan and R. Chen, *Sci. Rep.*, 2015, **5**, 8470.
5 R. Randler, M. Dietterle and D. M. Kolb, *Z. Phys. Chem.*, 1999, **208**, 43–56.
6 C. Xue, J. E. Millstone, S. Li and C. A. Mirkin, *Angew. Chem., Int. Ed.*, 2007, **46**, 8436–8439.
7 S. K. Srivastava, T. Hasegawa, R. Yamada, C. Ogino, M. Mizuhata and A. Kondo, *RSC Adv.*, 2013, **3**, 18367–18372.
8 R. J. Randler, D. M. Kolb, B. M. Ocko and I. K. Robinson, *Surf. Sci.*, 2000, **447**, 187–200.
9 J. G. Xu and X. W. Wang, *Surf. Sci.*, 1998, **408**, 317–325.
10 D. Krznarić and T. Goričnik, *Langmuir*, 2001, **17**, 4347–4351.
11 A. H. Pakiari and Z. Jamshidi, *J. Phys. Chem. A*, 2010, **114**, 9212–129221.
12 T. Trimble, L. Tang, N. Vasiljevic, N. Dimitrov, M. van Schilfgaarde, C. Friesen, C. V. Thompson, S. C. Seel, J. A. Floro and K. Sieradzki, *Phys. Rev. Lett.*, 2005, **95**, 166106.
13 O. M. Magnussen and R. J. Behm, *J. Electroanal. Chem.*, 1999, **467**, 258–269.
14 F. Grillo, H. Früchtl, S. M. Francis and N. V. Richardson, *New J. Phys.*, 2011, **13**, 013044.
15 Y. Xia, Y. Xiong, B. Lim and S. E. Skrabalak, *Angew. Chem., Int. Ed.*, 2009, **48**, 60–103.
16 M. Tsuji, D. Yamaguchi, M. Matsunaga and M. J. Alam, *Cryst. Growth Des.*, 2010, **10**, 5129–5135.
17 Y. Yoshida, K. Uto, M. Hattori and M. Tsuji, *CrystEngComm*, 2014, **16**, 5672–5680.
18 B. Radha, M. Arif, R. Datta, T. Kundu and G. Kulkarni, *Nano Res.*, 2010, **3**, 738–747.
19 B. Radha and G. U. Kulkarni, *Cryst. Growth Des.*, 2011, **11**, 320–327.
20 G. Mettela and G. U. Kulkarni, *Nano Res.*, 2015, **8**, 2925–2934.
21 S. Kiruthika, R. Gupta, K. D. M. Rao, S. Chakraborty, N. Padmavathy and G. U. Kulkarni, *J. Mater. Chem. C*, 2014, **2**, 2089–2094.
22 T. Ogura, M. Malcomson and Q. Fernando, *Langmuir*, 1990, **6**, 1709–1710.
23 M. Enyo, *J. Electroanal. Chem. Interfacial Electrochem.*, 1985, **186**, 155–166.
24 M. Tsuji, D. Yamaguchi, M. Matsunaga and K. Ikedo, *Cryst. Growth Des.*, 2011, **11**, 1995–2005.
25 J. T. Miller, A. J. Kropf, Y. Zha, J. R. Regalbuto, L. Delannoy, C. Louis, E. Bus and J. A. van Bokhoven, *J. Catal.*, 2006, **240**, 222–234.
26 W. J. Huang, R. Sun, J. Tao, L. D. Menard, R. G. Nuzzo and J. M. Zuo, *Nat. Mater.*, 2008, **7**, 308–313.
27 T. W. Janssens, B. Clausen, B. Hvolbæk, H. Falsig, C. Christensen, T. Bligaard and J. Nørskov, *Top. Catal.*, 2007, **44**, 15–26.
28 Y.-H. Lee, G. Kim, M. Joe, J.-H. Jang, J. Kim, K.-R. Lee and Y.-U. Kwon, *Chem. Commun.*, 2010, **46**, 5656–5658.
29 H. Oyanagi, Y. Orimoto, K. Hayakawa, K. Hatada, Z. Sun, L. Zhang, K. Yamashita, H. Nakamura, M. Uehara, A. Fukano and H. Maeda, *Sci. Rep.*, 2014, **4**, 7199.
30 J. Zeng, J. Tao, D. Su, Y. Zhu, D. Qin and Y. Xia, *Nano Lett.*, 2011, **11**, 3010–3015.
31 L. Zhang, H. Su, M. Sun, Y. Wang, W. Wu, T. Yu and J. Zeng, *Nano Res.*, 2015, **8**, 2415–2430.
32 M. Liu, Y. Zheng, L. Zhang, L. Guo and Y. Xia, *J. Am. Chem. Soc.*, 2013, **135**, 11752–11755.
33 Y. Q. Wang, K. Nikitin and D. W. McComb, *Chem. Phys. Lett.*, 2008, **456**, 202–205.
34 A. F. Alvarez Paneque, B. Rodriguez Gonzalez, I. Pastoriza-Santos and L. M. Liz-Marzan, *J. Phys. Chem. C*, 2013, **117**, 2474–2479.